Supplementary Material and Methods

Bulk RNA-Seq and analysis

Global transcriptome profiling was performed by RNA-seq in LX2 cells treated with either scramble RNA (siNT) or small interfering RNA targeting either YAP (siYAP) or TAZ (siTAZ) for 7 days. Total RNA was extracted using Trizol reagent following the manufacturer's instructions. mRNA library preparation (poly A enrichment) was performed by Novogene using Illumina NovaSeq PE150 platform. Resulting raw data was processed by following procedures: trim off adapter and low-quality reads using Trim_galore, reads aligned to the reference genome using STAR (mm10_STAR_genome_idx), Samtools index sorted bam files, Picard removed duplicates and HTSeq for quantification of the gene expression data. Differential expression genes (DEG) were performed using Deseq, and pathway gene enrichment was analyzed by gene set enrichment analysis (GSEA) software. The RNA-seq raw datasets and gene counts have been uploaded to the National Center for Biotechnology Information (NCBI) Gene Expression Omnibus database (GSE219088).

Single cell RNA-seq analysis

The CellRanger processed barcodes, features and matrix files of the single cell RNA-seq data for the CCl4 and BDL models was downloaded from GEO with the accession number GSE171904. The R package Seurat (Version 4.2.1) was used for downstream analysis. (1) Briefly, the Seurat objects of CCl4 and BDL were filtered based on the condition that percent.mt < 15% and 200< nFeature_RNA < 4000. Then the Seurat objects were integrated by nfeatures=1000, and then the top 30 principal components were used to run UMAP and find clusters with a resolution at 0.2. Cell marker genes “Des”, “Pecam1”, “Adgre1”, “Ptprc”, “Krt19”, “Sox9”, “Mfap4”, “Alb”, “Cd3e” were used to label the identity of liver cells. The Des high cells were marked as HSC and were separated. The senescence, SASP, apoptosis and ferroptosis related genes were then queried on the HSC cells, and their related expression levels were plotted as violin plots and feature plot. To perform the gene set enrichment analysis on the HSC clusters, the R package escape was used. (2) Specifically, the enrichIt() function was called by performing the ssGSEA, and the resulting enrichment score was plotted by dittoSeq. (3)

GSEA analysis

Bulk RNA-seq data from isolated HSC from LratCre pos YAP f/f and YAP f/f from injured liver were downloaded from GSE212047. The raw fastq file were aligned to mm10 as the reference genome by hisat2 and the duplicated sequencing reads were removed by the command picard.jar MarkDuplicates. (4) The gene count tables were generated by htseq-count. (5) The resulted gene count tables were used as input for DESeq2,(6) and the customized rank tables for GSEA were created based on the ranking of -log10(pvalue)*sign(logFC). The mouse gene symbols were converted to the human gene symbols based on the gene orthology file HMD_HumanPhenotype.rpt downloaded from the MGI database. The GSEA software V4.1.0 (7, 8) with the self-curated pathway.gmt files were used to perform GSEA to the customized rank table with permutation of 1000.

Cell culture studies

The human MF-HSC line (LX2, from Scott Friedman, Mount Sinai School of Medicine) and primary HSCs from de-identified human liver explants and $Yap1^{flox/flox}$ mice were studied. Mouse primary HSCs were isolated by sequential digestion of the liver with pronase (Roche Diagnostics, Indianapolis, IN) and collagenase (Roche) followed by density gradient centrifugation, as described before. (9) HSCs were immediately cultured, treated with control adenovirus (Ad) expressing GFP or Cre recombinase on culture day 1, and harvested on culture day 7. The primary human HSCs were isolated using density gradient centrifugation method following previously published studies.(10-13) Briefly, human liver explants were perfused with collagenase in PBS and then gently minced; the resultant liver cell suspension was filtered through with a 100 μm strainer and then centrifuged at 50 × g for 2 min to remove hepatocytes. The non-parenchymal cell-enriched suspension were then resuspended in cold GBSS-NaCl solution containing 13.2 μg/mL type I DNase and centrifuged at 1700 rpm for 8 min. The obtained cell pellets were resuspended and gently mixed with density gradient Histodenz solution (Sigma-Aldrich), overlaid carefully with cold PBS, and centrifuged at 2500rpm for 17 min to attain the HSCs at the interface. Primary human HSCs were passaged three times to obtain homogeneous HSC populations that were then used for cell culture studies. HSCs were grown in Gibco® DMEM containing 10% FBS, and 1% penicillin-streptomycin (Life Technologies, Grand Island, NY). For P21 overexpression, LX2 cells were transfected with P21 plasmid

(Addgene #16240) using lipofectamine 3000 reagents (Thermo Fisher Scientific) according to manufacture instructions. For gene knockdown, cells were treated with 20nM ON-TARGETplus siRNA (Dharmacon) to either P21, YAP or TAZ using RNAiMax transfection reagent (Thermo Fisher). Overexpression or knockdown efficacy was validated by qRT-PCR and/or Western blot analysis. LX2 cells were treated with 2.5 ng/mL TGFβ for 48h to maximize myofibroblastic activity or with 250 nM etoposide for 7 days to induce senescence; erastin or RSL3 or cyst(e)inase were added to induce ferroptotic cell death; ABT-263 or A1331852 were used to induce senolytic cell death; results were compared to vehicle (0.01% DMSO)-treated cultures. In some cyst(e)inase-treated cultures, medium was supplemented with antioxidant NAC (2 mmol/L) or with ferroptosis inhibitor liproxstatin (0.5 μmol/L). Cell growth/viability was monitored with Cell Counting Kit-8 (CCK8, Dojindo Molecular Technologies). Before harvesting cells for RT-PCR and western blots, cell medium was removed and plates were washed twice with PBS. Cell nuclear and Cytoplasmic fraction were separated using the NE-PER™ Nuclear and Cytoplasmic Extraction Reagents following manufacturer's instruction (# 78833, Thermo Fisher).

Quantitative real time PCR (qRT-PCR)

Total RNA was isolated from whole liver tissue or cultured cells using Trizol reagent. After determining the concentration and quality of the RNA, complementary DNAs (cDNA) were generated using Superscript II Reverse Transcriptase (Life Technologies) according to the manufacturer's instructions. Each cDNA sample was assayed by qRT-PCR using SYBR Green Super-mix using primers listed in **Supplementary Table 1**. Results were normalized to the housekeeping gene S9 based on the threshold cycle (C_t) and relative fold change was determined using the $2^{-\Delta\Delta Ct}$ method.

Immunoblot analysis

Protein was extracted from isolated cell pellets or whole liver tissue using RIPA buffer with protease inhibitors (Sigma-Aldrich). Equal amounts of protein were loaded and separated by SDS-PAGE gel electrophoresis on 4%-20% Criterion gels (BioRad, Hercules, CA), and then transferred to PVDF membranes, and incubated with the following primary antibodies: αSMA (Abcam, ab32575), Vimentin (Abcam, 92547), Collagen I (Cell signaling, 84336), YAP and TAZ (Cell signaling, 8418), Phospho-YAP (Cell signaling, 4911), CyclinD1 (Abcam, ab134175), CyclinA2 (ab181591), GPX4 (Abcam, ab125066), P21

(ab188224 or Cell signaling, 2947), or β-tubulin (Abcam, ab6046). Blots were visualized with HRP-conjugated secondary antibodies.

Histopathological analysis, Immunohistochemistry (IHC) and Immunocytochemistry (ICC)

Liver tissue was fixed in formalin, embedded in paraffin, and cut into sections. The slides were stained with H&E and evaluated for hepatocyte injury. Liver fibrosis was assessed by Picrosirius red (#365548, Sigma) staining according to the manufacturer's suggestions. Terminal deoxynucleotidyl transferase dUTP nick end labeling (TUNEL) staining was performed for cell death using the In Situ Cell Death Detection Kit, AP (Roche Diagnostics, Indianapolis, IN) following manufacturer's instructions. For IHC, slides were dewaxed, hydrated, and incubated for 10 min in 3% hydrogen peroxide to block endogenous peroxidase. Antigen retrieval was performed by heating in 10 mmol/L sodium citrate buffer (pH 6.0) for 10 min. Sections were blocked in Dako protein block solution (X090, Agilent Technologies, Santa Clara, CA) for 1hr and incubated OVN at 4°C with indicated primary antibodies: αSMA (Abcam, ab32575); YAP (Cell signaling, 14074 or 8418); p-YAP (Cell signaling, 13008); P21 (Abcam, ab188224); Desmin (Abcam, ab15200); CK-19 (Abcam, ab133496); CK-19 (Santa Cruz, sc-70936). Polymer-horseradish peroxidase secondary antibodies were applied for 1h at room temperature, and Dako *3,3′-Diaminobenzidine* Substrate Chromogen System was used for detection. For fluorescence detection, Alexa Fluor™ 488 and Alexa Fluor™ 594 secondary antibodies were used and images were acquired and processed using Leica Microsystems. Frozen liver tissue samples were also used and cut at 10uM thickness, fixed with 10% formalin, and stained with Oil Red O (Sigma, O0625-25G) for 10 min. Cellular senescence in liver was evaluated by SA-β-gal staining using a commercially available kit (Cell Signaling, #9860) and followed the manufacturer's instruction. For SA-β-gal and desmin co-staining, frozen sections were firstly stained for SA-β-gal, blocked in Dako protein block solution, and further incubated with Desmin antibody (Abcam, ab15200) following the IHC procedure described above. Results were examined by light microscopy. For ICC, cells were washed, fixed in 4% paraformaldehyde, permeabilized, blocked with normal goat serum, and incubated overnight with YAP antibody (Cell signaling, 14074). Cells were washed in PBS and incubated with Alexa Fluor 488 goat anti-rabbit IgG (H+L, ThermoFisher Scientific) for 1h at RT. 4',6-diamidino-2-phenylindole (*DAPI*) was used to visualize nuclei. Images were acquired and processed using a Zeiss LSM710 inverted confocal microscope system.

Statistics

Data were expressed as mean ± SEM. Statistical significance between two groups was evaluated using the student's t test, while comparisons of multiple groups were assessed by one-way analysis of variance (ANOVA), followed by Student–Newman–Keul's test. $p \leq 0.05$ was considered to be statistically significant.

Supplementary Table 1. Primer used for qRT-PCR

	Gene symbol	Primer Forward	Primer Reverse
Human	*S9*	GACTCCGGAACAAACGTGAGGT	CTTCATCTTGCCCTCGTCCA
	Acta2 (αSma)	GGAGATCACGGCCCTAGCAC	AGGCCCGGCTTCATCGTAT
	Col1a1 (Col1α1)	CGGTGTGACTCGTGCAGC	ACAGCCGCTTCACCTACAGC
	Desmin	CAGTGGCTACCAGGACAACA	GCTGGTTTCTCGGAAGTTGA
	YAP	CAGACAGTGGACTAAGCATGAG	CAGGGTGCTTTGGTTGATAGTA
	TAZ (WWTR1)	GAAGGTGATGAATCAGCCTCTG	GTTCTGAGTCGGGTGGTTCTG
	CDKN1A (P21)	GACACCACTGGAGGGTGACT	CAGGTCCACATGGTCTTCCT
	CDKN1A (P16)	CCAACGCACCGAATAGTTACG	GCGCTGCCCATCATCATG
	CSF2	GGCCCCTTGACCATGATG	TCTGGGTTGCACAGGAAGTTT
	CXCL1	GAAAGCTTGCCTCAATCCTG	CACCAGTGAGCTTCCTCCTC
	CXCL2	AACTGCGCTGCCAGTGCT	CCCATTCTTGAGTGTGGCTA
	IL6	CCGGGAACGAAAGAGAAGCT	GCGCTTGTGGAGAAGGAGTT
	IL7	CTCCAGTTGCGGTCATCATG	GAGGAAGTCCAAAGATATACCTAAAAGAA
	IL8	CTTTCCACCCCAAATTTATCAAAG	CAGACAGAGCTCTCTTCCATCAGA
	HMGA1	AGGAGCAGTGACCCATGCGT	TGATGGTGGGCCTGGGGAAG
	CTGF	CTCCACCCGGGTTACCAATG	CTTCCAGGTCAGCTTCGCAA
	ANKRD1	AGTAGAGGAACTGGTCACTGG	TGGGCTAGAAGTGTCTTCAGAT
	CYR61	GGGCTGGAATGCAACTTC	TACAGTTGGGCTGGAAACT
	GPX4	GCCTTCCCGTGTAACCAGT	GCGAACTCTTTGATCTCTTCGT
	CyclinD1	TATTGCGCTGCTACCGTTGA	CCAATAGCAGCAAACAATGTGAAA
	CyclinA2	TTATTGCTGGAGCTGCCTTT	CTCTGGTGGGTTGAGGAGA
	FOXM1	GACTTCTTGGGTCTTGGGGT	GGAGGAAATGCCACACTTAGCG
Mouse	*S9*	GGGCCTGAAGATTGAGGATT	CGGGCATGGTGAATAGATTT
	Col1a1 (Col1α1)	GAGCGGAGAGTACTGGATCG	GCTTCTTTTCCTTGGGGTTC
	Col3a1 (Col3α1)	GGTTTCTTCTCACCCTTCTTC	CTTCCAGACATCTCTAGACTCA
	Col6a1 (Col6α1)	CGACTGCGCCATTAAGAAG	CGGTCACCACGATCAAGTA
	IL6	TGATTGTATGAACAACGATGATGC	GGACTCTGGCTTTGTCTTTCTTGT
	Cxcl1	CTGGGATTCACCTCAAGAACATC	CAGGGTCAAGGCAAGCCTC
	IL1 β	CCACCTCAATGGACAGAATATCA	CCCAAGGCCACAGGTATTT
	PDGFR-β	GACTACCTGCACCGGAACAA	GTCCAACATGGGCACGTAA
	Yap1	AGCAGCAGCAAATACAGCTGCAG	AGCATTTGCTGTGCTGGGATTGA
	Acta2 (αSma)	GCCAGTCGCTGTCAGGAACCC	AGCCGGCCTTACAGAGCCCA
	Desmin	TACACCTGCGAGATTGATGC	ACATCCAAGGCCATCTTCAC
	Vim (Vimentin)	GCCGAAAGCACCCTGCAGTCA	TGGGCCTGCAGCTCCTGGAT
	Ctgf	TGACCTGGAGGAAAACATTAAGA	AGCCCTGTATGTCTTCACACTG
	Ankrd1	GGAACAACGGAAAAGCGAGAA	GAAACCTCGGCACATCCACA
	Cyr61	GGGCTGGAATGCAACTTC	TACAGTTGGGCTGGAAACT
	Areg	CCATCATCCTCGCAGCTATT	CCATCATCCTCGCAGCTATT
	Ck7	TAGAGTCCAGCATCGCAGAG	CACAGGTCCCATTCCGTC
	Ck19	CATGGTTCTTCTTCAGGTAGGC	GCTGCAGATGACTTCAGAACC
	Ccl5	CCCTCACCATCATCCTCACT	GCACTTGCTGCTGGTGTAGA
	IFN--β	GTTACACTGCCTTTGCC	AATAGTCTCATTCCACCC
	IL10	TGGACTCCAGGACCTAGACAG	AGGACACCATAGCAAAGGGC

Supplemental figure legends.

Suppl. Fig. 1 Cell-to-cell contact regulates ferroptosis sensitivity of HSCs. LX2 cells grown at low density (< 30% confluence) or high density (100% confluence) were treated with erastin or RSL3 for 48h. Phase pictures were taken at 40x magnification.

Suppl. Fig. 2 YAP depletion suppresses HSC ferroptosis susceptibility. LX2 cells were treated with scrambled RNA (siNT) or small interfering RNA targeting either YAP (siYAP) or TAZ (siTAZ) for 3 days, and then treated with erastin **(A)** or RSL3 **(B)** for another 2 days. Phase pictures were taken at 100x magnification.

Suppl. Fig. 3 TGFβ signaling increases ferroptosis susceptibility of HSCs in a YAP-dependent manner. LX2 cells were first treated with TGFβ for 48h, followed with 2uM erastin for another 48h. Phase pictures were taken at 40x magnification.

Suppl. Fig. 4 Hippo-YAP pathway mediates ferroptosis sensitivity of HSCs by regulating P21-GPX4 axis. Expression of YAP or TAZ was knocked-down by siRNA, and cells were then harvested for bulk RNA-seq. **(A)** Differential expression analysis shows that YAP deficiency affects the expression of many more genes than TAZ deficiency. Dots colored in red represent transcripts that are significantly up- or down-regulated ($p<0.01$). **(B)** Volcano plot reveals that P21 is one of the most upregulated genes when YAP is knocked down.

Suppl. Fig. 5 YAP deficiency induces HSC senescence. LX2 cells were treated with scrambled RNA (siNT) or small interfering RNA targeting either YAP (siYAP) or TAZ (siTAZ) for 7 days. **(A, B)** GSEA of transcriptomes revealed that depleting YAP enriched gene signatures of cellular senescence and many senescence-associated pathways. **(C, D, E)** YAP deficiency decreased cell growth, upregulated senescent markers p16, p21 but decreased proliferation markers CYCLINA2 and FOXM1. **(F)** GSEA of transcriptomes revealed that depleting YAP enriched gene signatures of apoptosis pathway. **(G)** Primary human HSC expressed typical markers HSCs. **(H)** YAP and TAZ deficiency caused cell cycle arrest in primary human HSCs. Data are graphed as mean ± sem of n=3-5 samples/group. *$p<0.05$ vs siNT. $^{\#}p<0.05$ vs siYAP and siTAZ.

Suppl. Fig. 6 YAP signature is the top downregulated gene signature in senescent or "deactivated" HSCs. (A, B) GSEA of 2 published RNA-seq datasets comparing primary human "senescent HSCs to growing HSCs (GSE11954)" or "reverted HSCs to activated HSCs (GSE68001)" identified Cordenonsi_YAP_conserved_signature is the top-downregulated gene-set in senescent or deactivated HSCs, respectively. **(C, D)** GSEA plot of the Cordenonsi_YAP_conserved_signature. **(E, F)** Heatmap of the gene list in the Cordenonsi_YAP_conserved_signature. Several canonical YAP targeted genes are highlighted.

Suppl. Fig. 7 Senescent HSCs are less proliferative and fibrogenic. (A-C) LX2 cells were treated with 250nM etoposide for 7 days to induce HSC senescence. Senescent HSCs exhibited reduced expression of proliferation markers and MF-HSC markers. *p<0.05 vs ctrl. **(D, E)** P21 overexpression (OE) by P21 plasmid vector reduced expression of proliferation markers and MF markers. *p<0.05 vs ctrl empty vector. Data are graphed as mean ± sem of n=4-5 samples/group.

Suppl. Fig. 8 Identification of HSC population by cell type specific markers. The single cell RNA-seq data for HSCs from the CCl_4 and BDL models was downloaded from GEO with the accession number GSE171904. The Seurat objects were filtered based on the condition that percent.mt < 15% and 200< nFeature_RNA < 4000. Then the Seurat objects were integrated by nfeatures=1000, and the top 30 principal components were used to run UMAP and find clusters with a resolution at 0.2. HSC identify was indicated by gene markers Des, Lrat, Acta 2 and Col1a1.

Suppl. Fig. 9 HSC sub-clustering and further pathway and individual gene profiling. (A) UMAP visualization of 7 distinct HSC clusters. **(B)** ssGSEA gene set enrichment analysis was performed on the HSC clusters, and the resulting enrichment score was plotted by dittoSeq. **(C)** DotPlot visualization of cell phenotype markers. Dot size reflects percentage of cells in a cluster expressing each gene; dot color reflects expression level.

Suppl. Fig. 10 HSCs are highly susceptible to cyst(e)inase-induced ferroptosis. (A) LX2 cells were treated with cyst(e)inase for 48h, and cell viability was measured by CCK8 assay. In some cells, the

culture medium was supplemented with either 0.5uM liprostatin or 2mM NAC. **(B)** Phase pictures were taken at 40x magnification. Data are graphed as mean ± sem of n=4 assays/group. *p<0.05 vs ctrl.

Suppl. Fig. 11 A subset of HSCs undergo senescence during liver fibrosis. Mice were treated with CCl_4 or its vehicle (corn oil) for 6 weeks. **(A)** SA-β-gal & Desmin co-staining in OCT-embed liver tissues from healthy or CCl_4-treated mice, some double positive cells are indicated by arrows. **(B)** p21 & desmin co-immunostaining in paraffin-embed liver tissues from healthy or CCl_4-treated mice. **(C)** Normalized p21 gene count in a published bulk RNA-seq dataset of primary HSCs (GSE134512) isolated from CCl_4 or vehicle-treated livers. Data are graphed as mean ± sem of n=3 samples/group. *p<0.05 vs vehicle ctrl.

Suppl. Fig. 12 Selective YAP depletion in MF-HSC induces senescence and protects against liver fibrosis. (A) Primary HSCs were harvested from $YAP^{flox/flox}$ mice and then treated with control adenovirus expressing GFP or adenovirus harboring Cre recombinase. Compared with HSCs that were treated with AdGFP, AdCre significantly decreased expression of YAP, its target gene CTGF and MF marker αSMA. **(B-D)** αSMA-$CreER^{T2}$ x $Yap1^{flox/flox}$ mice were subjected to sham or BDL surgery for 14 days to promote MF-HSC accumulation and liver fibrosis. Tamoxifen or its vehicle corn oil was intraperitoneally administered every other day from day 4 until liver tissue was harvested. (B) mRNA expression of p21. (C) Protein expression of p21 and aSMA. (D) mRNA expression of CK7 and CK19. Data are graphed as mean ± sem of n=6-7 mice /group. $^{\#}p<0.05$ vs DTG -Veh.

Suppl. Fig. 13 Tamoxifen has minimal effects on hepatic YAP activity, senescence, liver injury, fibrosis or ductular reactions in single transgenic $Yap1^{flox/flox}$ mice. $Yap1^{flox/flox}$ mice were subjected to sham or BDL surgery for 14 days to promote MF-HSC accumulation and liver fibrosis. Tamoxifen or its vehicle corn oil was intraperitoneally administered every other day from day 4 until liver tissue was harvested. **(A)** TAM did not decrease expression of Yap1 or aSMA. **(B, C)** Tamoxifen did not significantly affect the expression of YAP target genes, p21 or indicated SASP factors. (**D**) Representative staining pictures to assess hepatic senescence (SA-β-Gal), liver histology (H&E), MF-HSC accumulation and liver fibrosis (Sirius Red, aSMA, desmin) and ductular reaction (CK7 and CK19). (**E**) Serum levels of ALT, AST and bilirubin to assess liver injury. **(F, G)** Quantification of the positive IHC positive area in staining of

Sirius Red, aSMA, desmin, CK7 or CK19. **(H)** mRNA expression of CK7 or CK19. Data are graphed as mean ± sem of n=5 mice /group in BDL mice. $^{\#}p<0.05$ vs STG -Veh.

Suppl. Fig. 14. Selective YAP depletion in MF-HSCs induces senescence and protects against MCD diet-induced liver injury and fibrosis. αSMA-CreER^{T2} x Yap1$^{flox/flox}$ mice were fed with MCD diet for 7 weeks, and tamoxifen or its vehicle corn oil was intraperitoneally administered every other day in the last 2 weeks. **(A, B, C)** tamoxifen decreased expression of Yap1 and its target gene Areg, but increased SASP factors. (**D**) Serum levels of ALT and AST. (**E**) Representative staining for assess hepatic senescence (SA-β-Gal), liver histology (H&E), MF-HSC accumulation and liver fibrosis (Sirius Red, aSMA). **(F)** Quantification of the IHC positive area in staining of Sirius Red and αSMA. Data are graphed as mean ± sem of n= 3 in chow fed mice and n=6 mice /group in MCD diet fed mice. *p<0.05 vs chow, $^{\#}p<0.05$ vs Yap1$^{flox/flox}$ mice.

Suppl. Fig. 15 Selective Yap1 deficiency in HSCs in fibrotic mice dramatically changed gene signatures involved in fibrogenesis, cell cycle, senescence, apoptotic and ferroptoic pathways. GSEA of transcriptomes of YAP $^{-/-}$ vs YAP $^{+/+}$ HSCs (LratCre x Yap1$^{flox/flox}$ vs Yap1$^{flox/flox}$) isolated from mice with chronic CCl_4-induced liver fibrosis (GSE212042).

Suppl. Fig. 1 Cell-to-cell contact regulates Hippo-YAP pathway and ferroptosis sensitivity of HSCs.

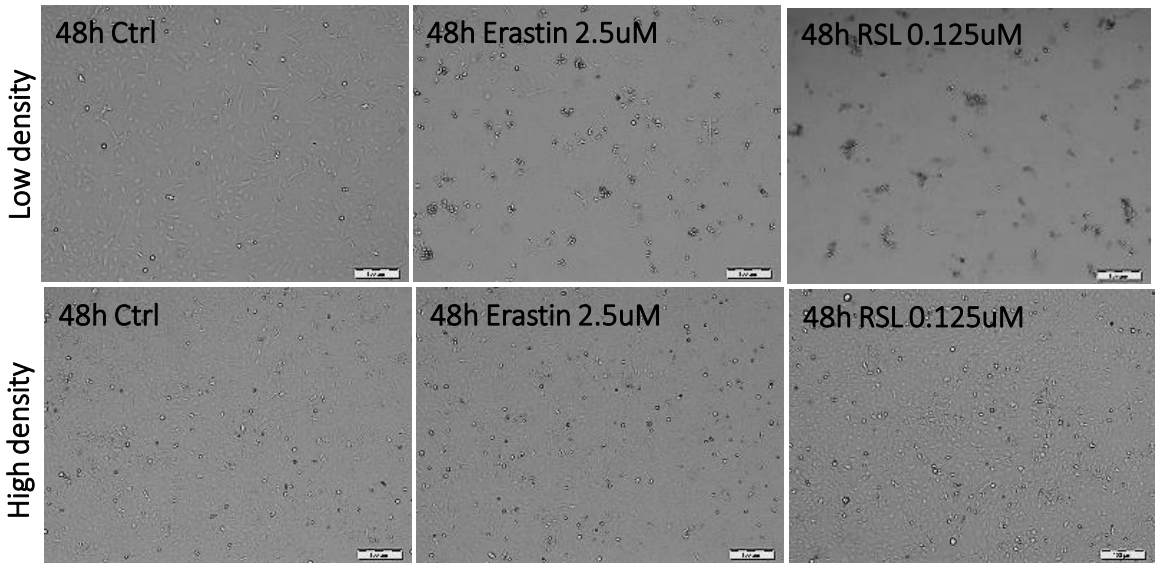

Suppl. Fig. 2 YAP depletion suppresses HSC myofibroblastic phenotype and ferroptosis susceptibility.

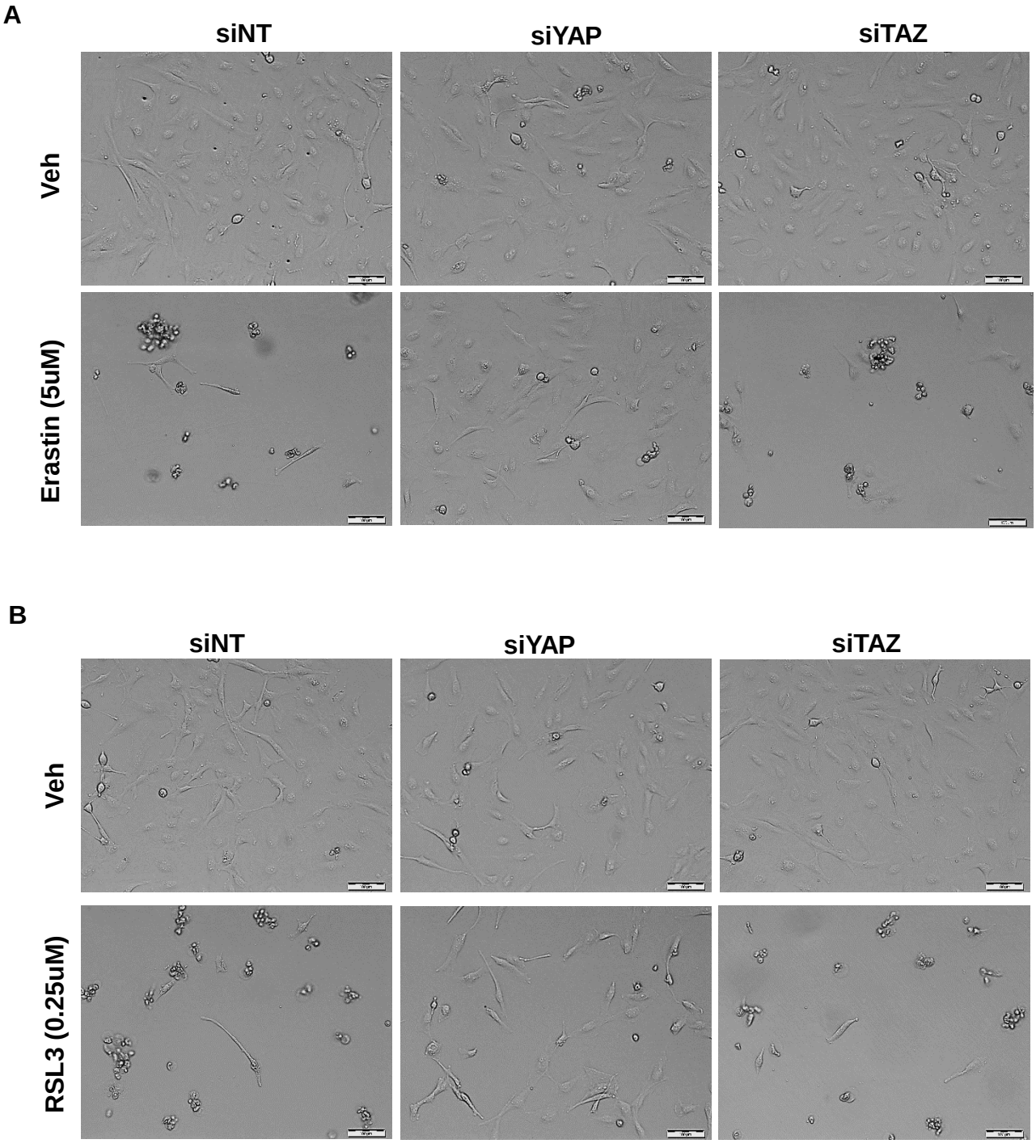

Suppl. Fig. 3 TGFβ signaling increases ferroptosis susceptibility of HSCs in a YAP-dependent manner.

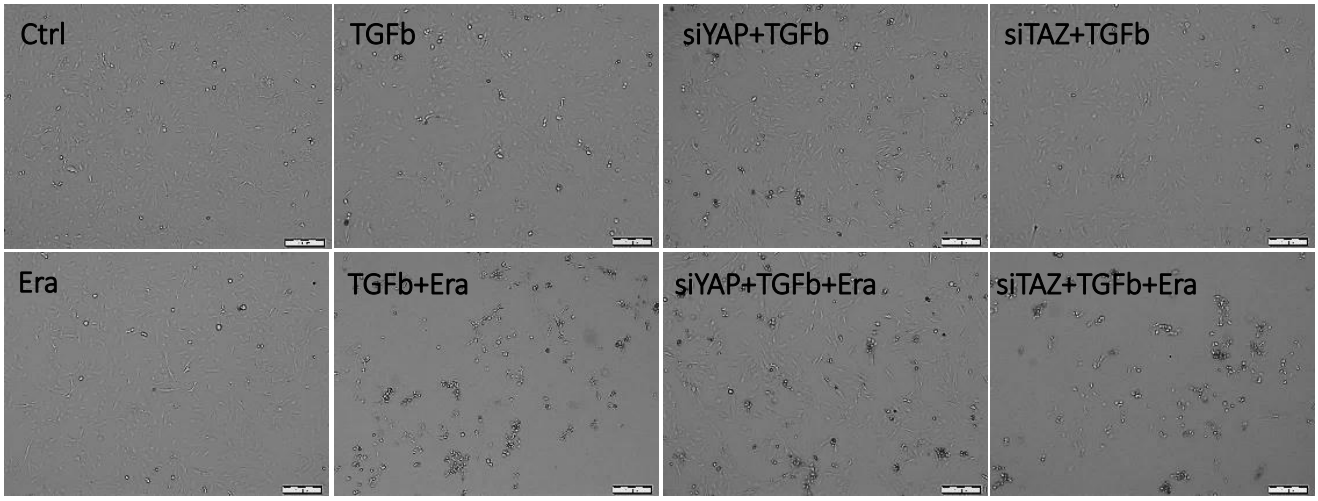

Suppl. Fig 4. YAP dictates MF-HSC ferroptosis sensitivity by regulating P21-GPX4 axis

A

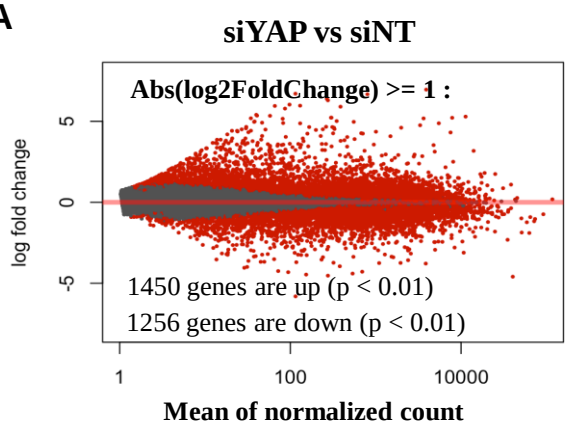

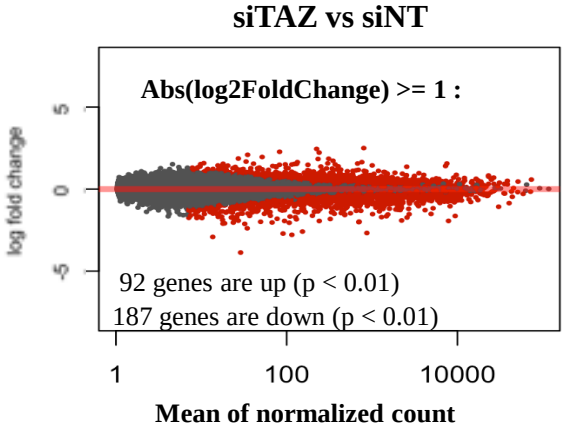

B

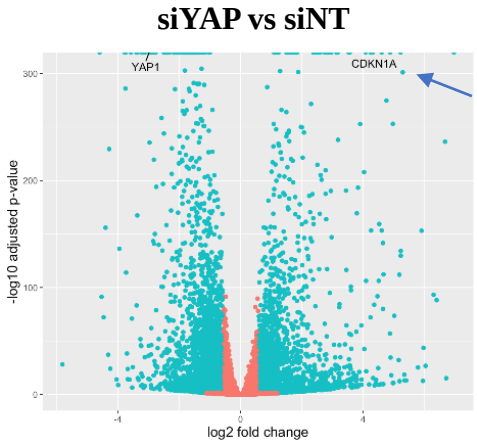

CDKN1A
log2FoldChange: 4.31
Adj p-value: < 1x10E-200

Suppl. Fig 5. YAP deficiency induces HSC senescence

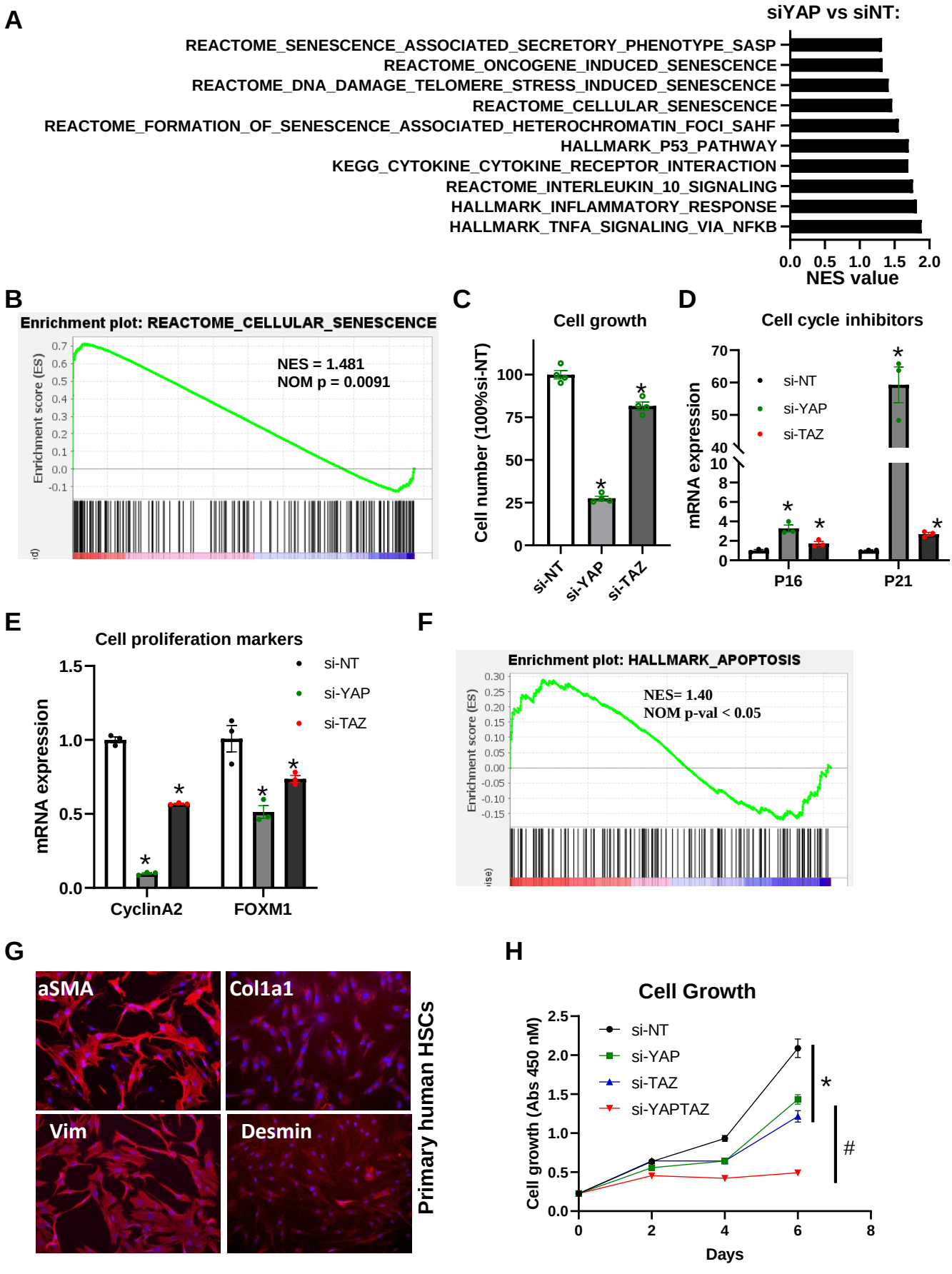

Suppl. Fig 6. YAP signature is the top downregulated gene signature in senescent or reverted HSCs

A

GSE11954 (etoposide in primary human HSCs)

	GS follow link to MSigDB	NES	NOM p-val	FDR q-val	FWER p-val
1	CORDENONSI_YAP_CONSERVED_SIGNATURE	-2.03	0.000	0.000	0.000
2	PRC2_EZH2_UP.V1_DN	-1.90	0.000	0.000	0.000
3	RPS14_DN.V1_DN	-1.79	0.000	0.000	0.001
4	GCNP_SHH_UP_LATE.V1_UP	-1.76	0.000	0.001	0.003
5	RB_P130_DN.V1_UP	-1.75	0.000	0.001	0.003
6	RB_P107_DN.V1_UP	-1.64	0.000	0.005	0.026
7	GCNP_SHH_UP_EARLY.V1_UP	-1.64	0.000	0.004	0.029
8	VEGF_A_UP.V1_DN	-1.62	0.000	0.005	0.039
9	P53_DN.V2_DN	-1.61	0.000	0.006	0.050
10	PRC2_EED_UP.V1_DN	-1.58	0.000	0.011	0.097

B

GSE68001 (EGF+FGF+FFA in primary human HSCs)

	GS follow link to MSigDB	NES	NOM p-val	FDR q-val	FWER p-val
1	CORDENONSI_YAP_CONSERVED_SIGNATURE	-2.51	0.000	0.000	0.000
2	RB_P107_DN.V1_UP	-2.45	0.000	0.000	0.000
3	ESC_V6.5_UP_EARLY.V1_DN	-2.32	0.000	0.000	0.000
4	RPS14_DN.V1_DN	-2.28	0.000	0.000	0.000
5	PRC2_EED_UP.V1_DN	-1.86	0.000	0.005	0.008
6	CSR_LATE_UP.V1_UP	-1.79	0.000	0.008	0.016
7	CAHOY_ASTROGLIAL	-1.73	0.000	0.009	0.022
8	PRC2_EZH2_UP.V1_DN	-1.70	0.000	0.012	0.033
9	RB_P130_DN.V1_UP	-1.65	0.008	0.015	0.048
10	P53_DN.V1_UP	-1.63	0.000	0.015	0.054

C

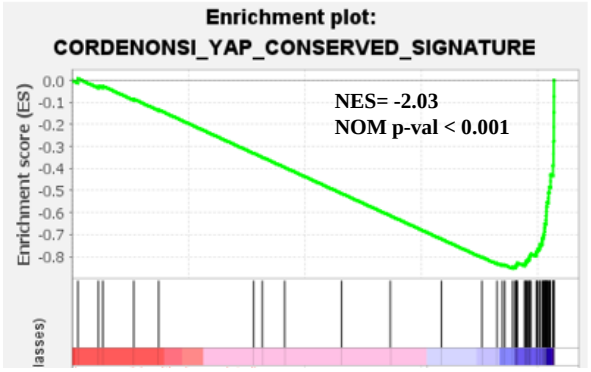

D

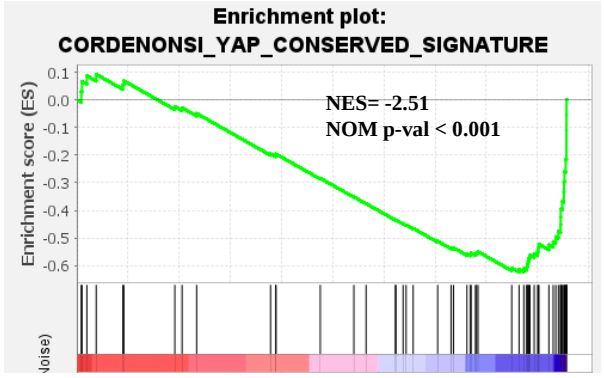

E

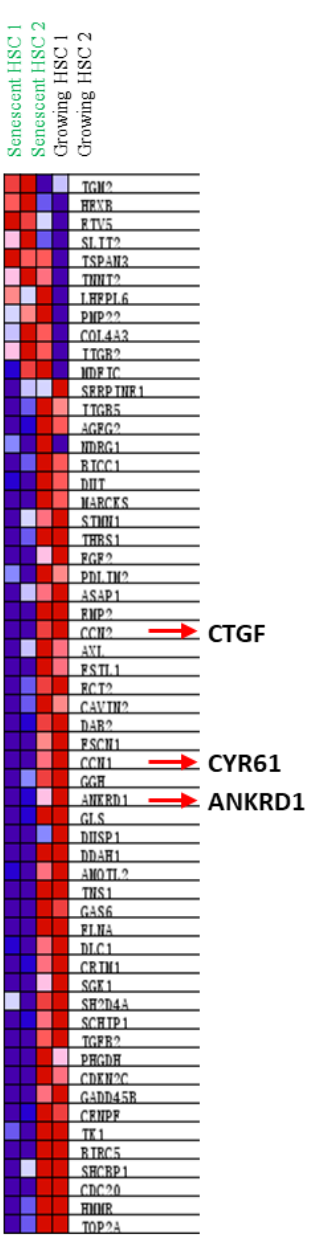

Gene profile of YAP signature (GSE11954)

F

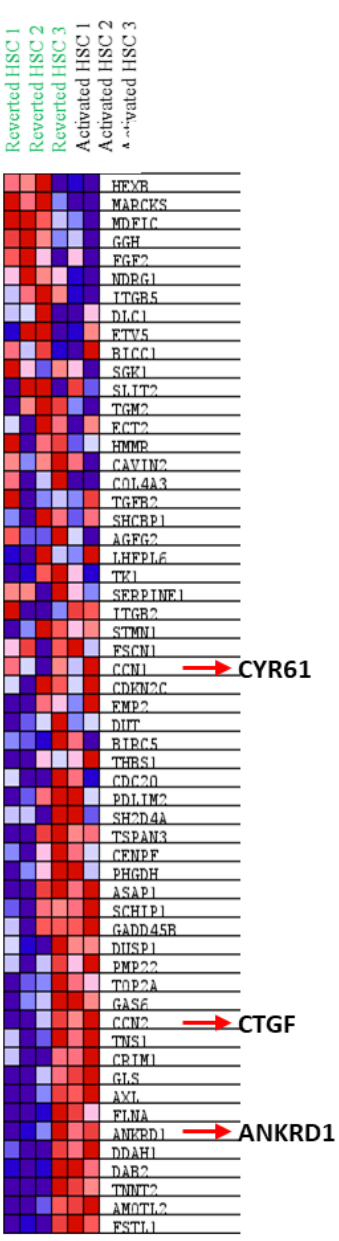

Gene profile of YAP signature (GSE68001)

Suppl. Fig 7. Senescent HSCs are less proliferative and fibrogenic

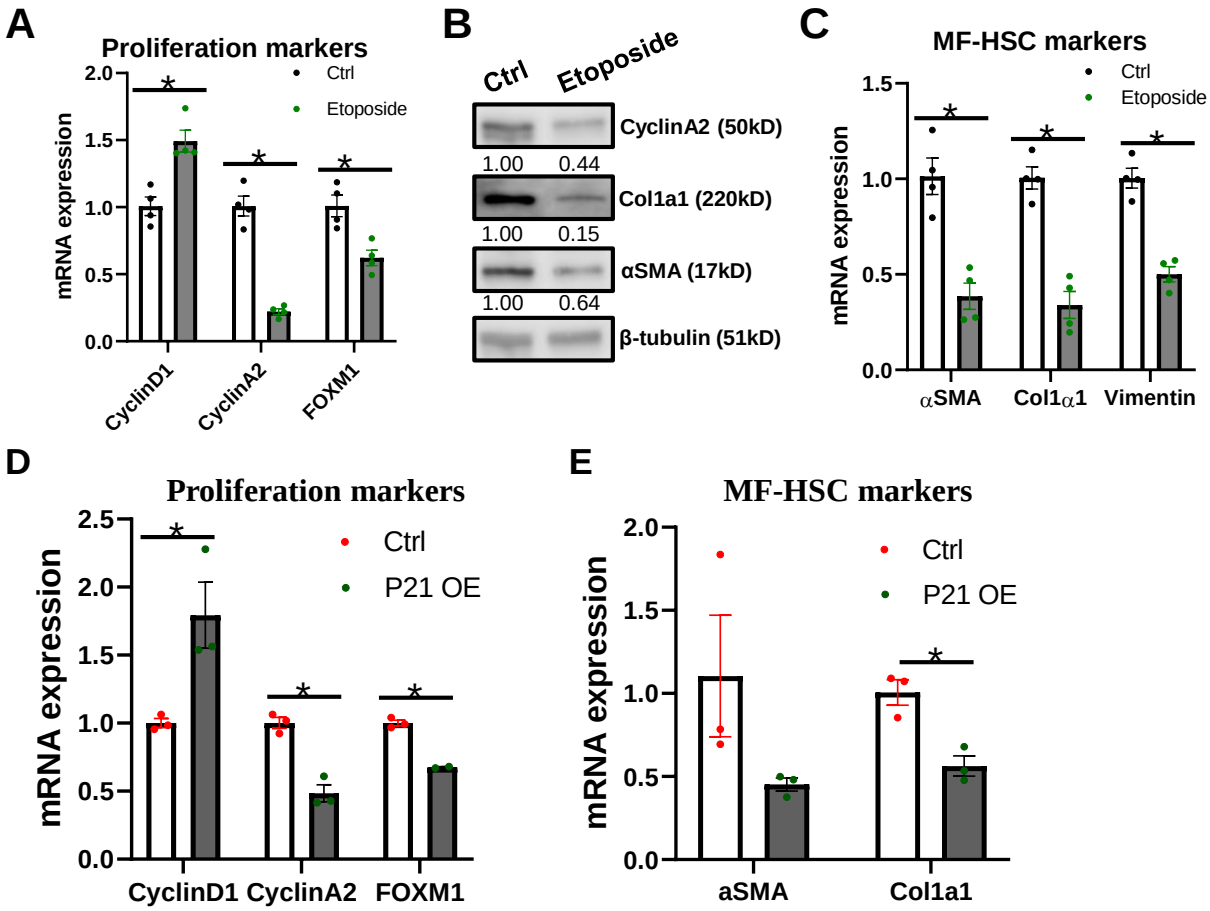

Suppl. Fig. 8 Identification of HSC population by cell type specific markers

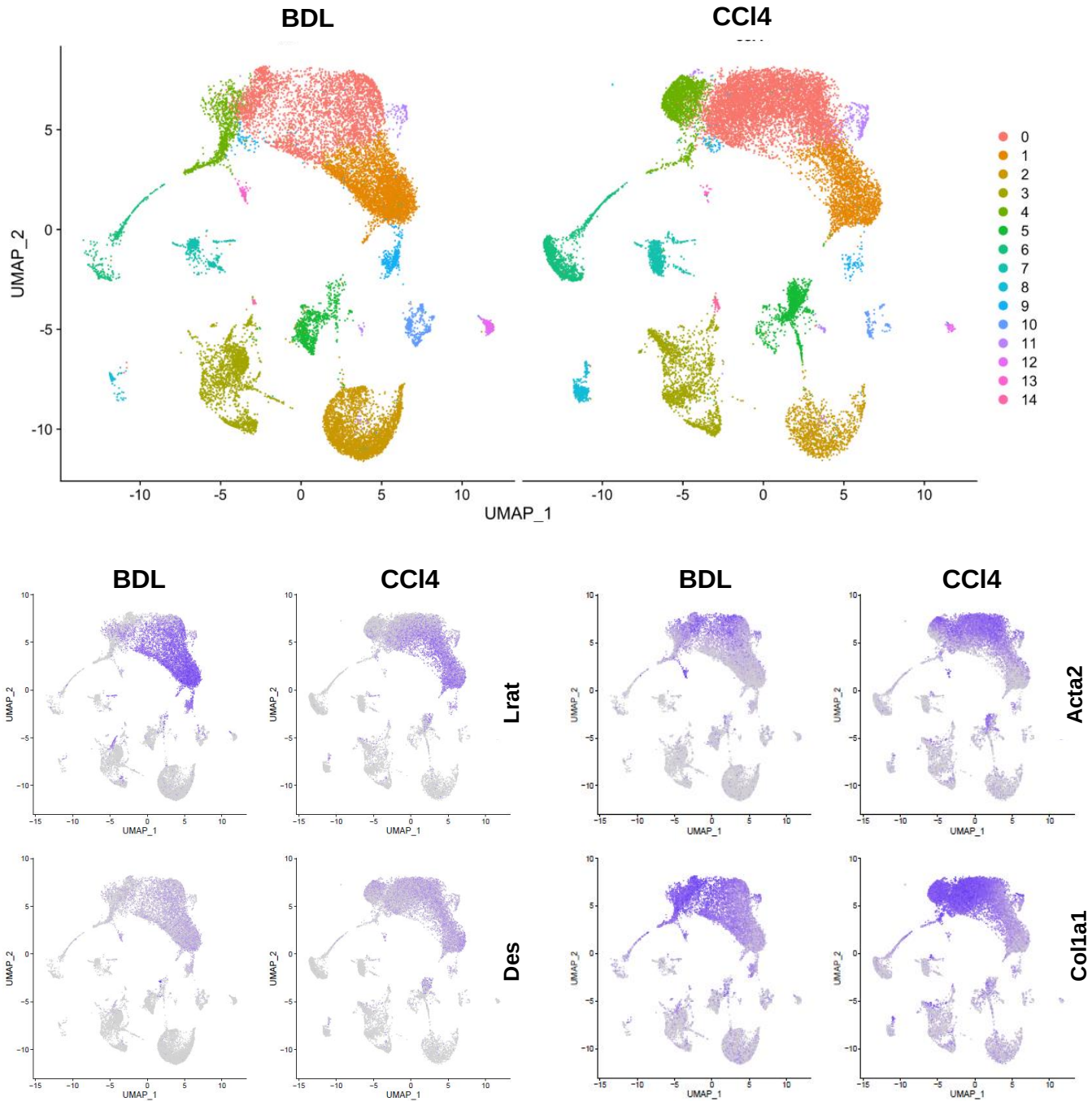

Suppl. Fig. 9 HSC sub-clustering for pathway and gene enrichment analysis

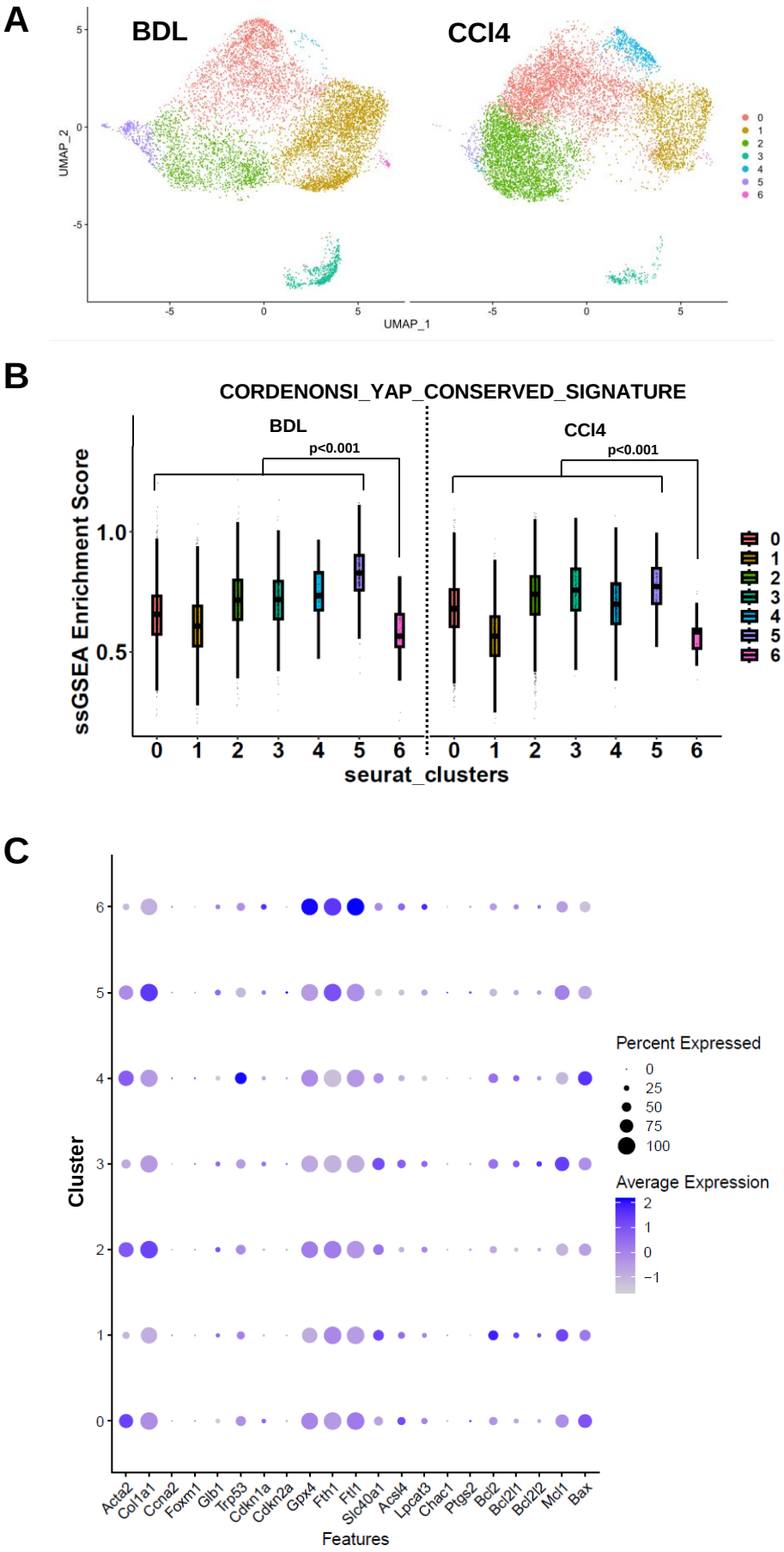

Suppl. Fig. 10 Cysteine depletion induces HSC ferroptosis

A

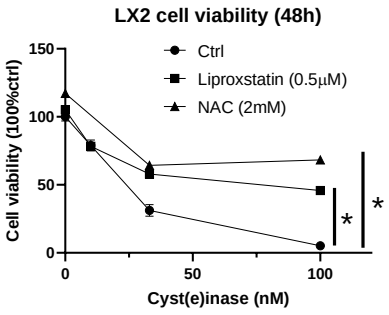

B

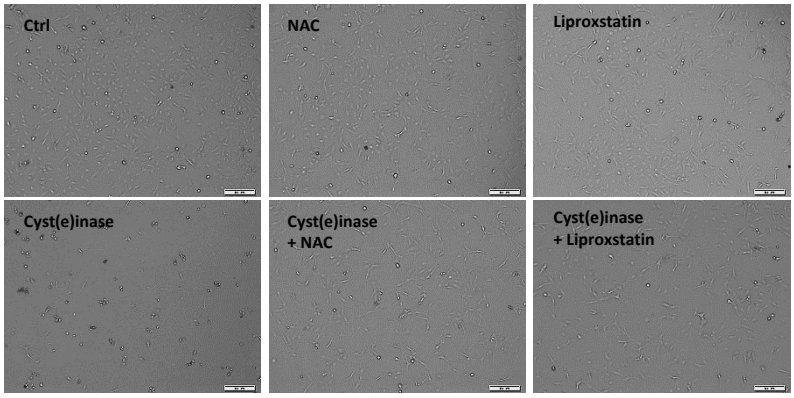

Suppl. Fig. 11 A subset of HSCs undergo cellular senescence during liver fibrosis

A

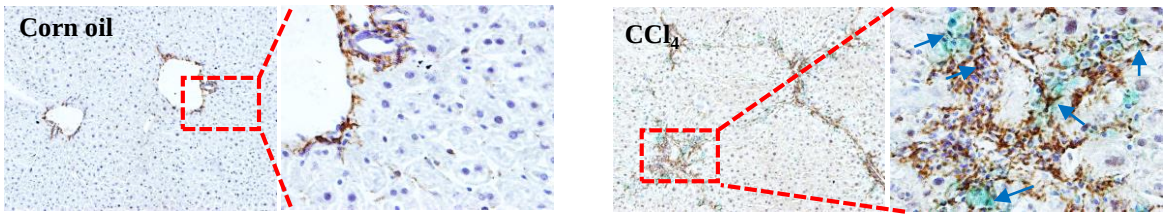

SA-β-Gal + Desmin staining

B

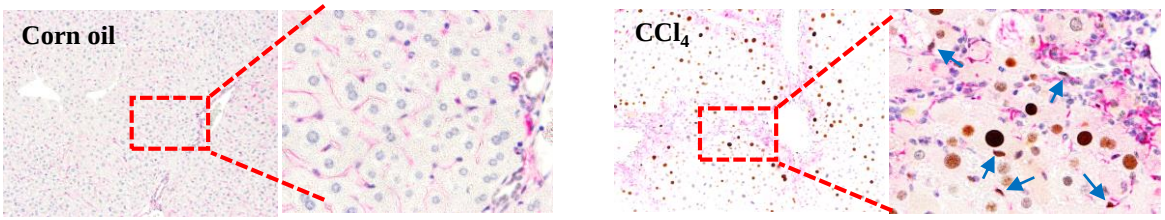

p21 + desmin staining

C

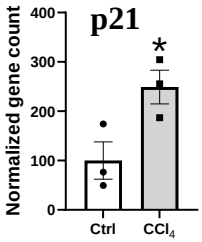

Isolated HSC from CCl4-treated mice

Suppl. Fig 12. Selective YAP depletion in MF-HSC induces senescence and protects against liver injury, fibrosis and ductulal reaction

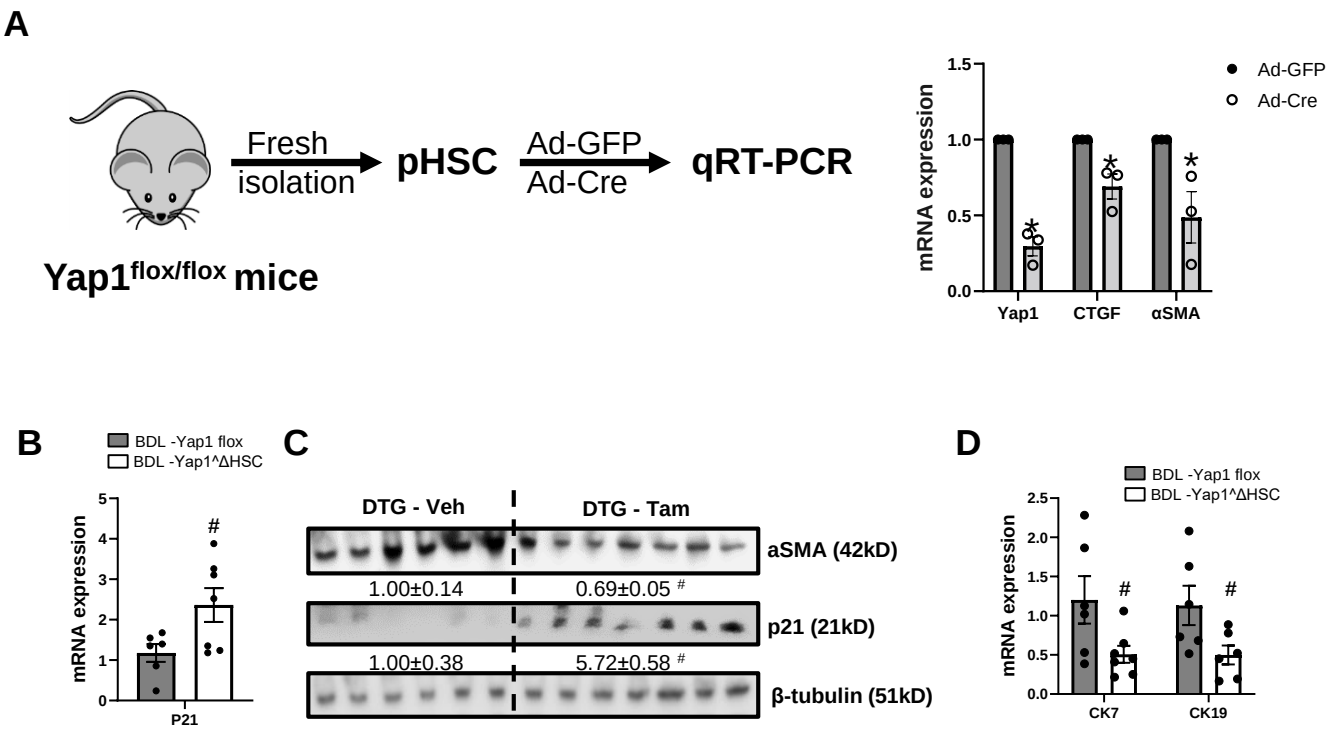

Suppl. Fig 13. Tamoxifen did not affect hepatic YAP activity, senescence, liver injury, fibrosis or ductular reaction in Yap1 flox mice

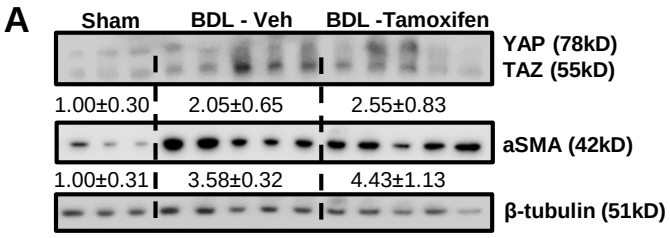

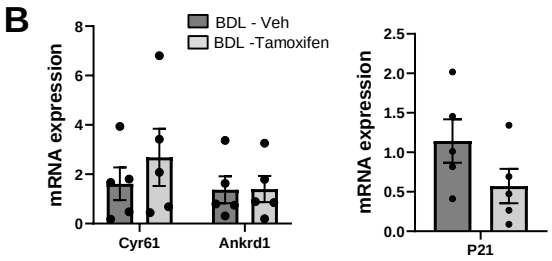

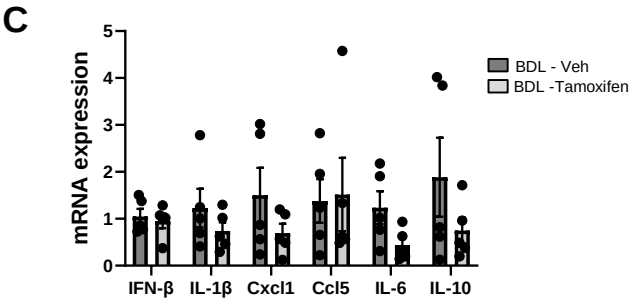

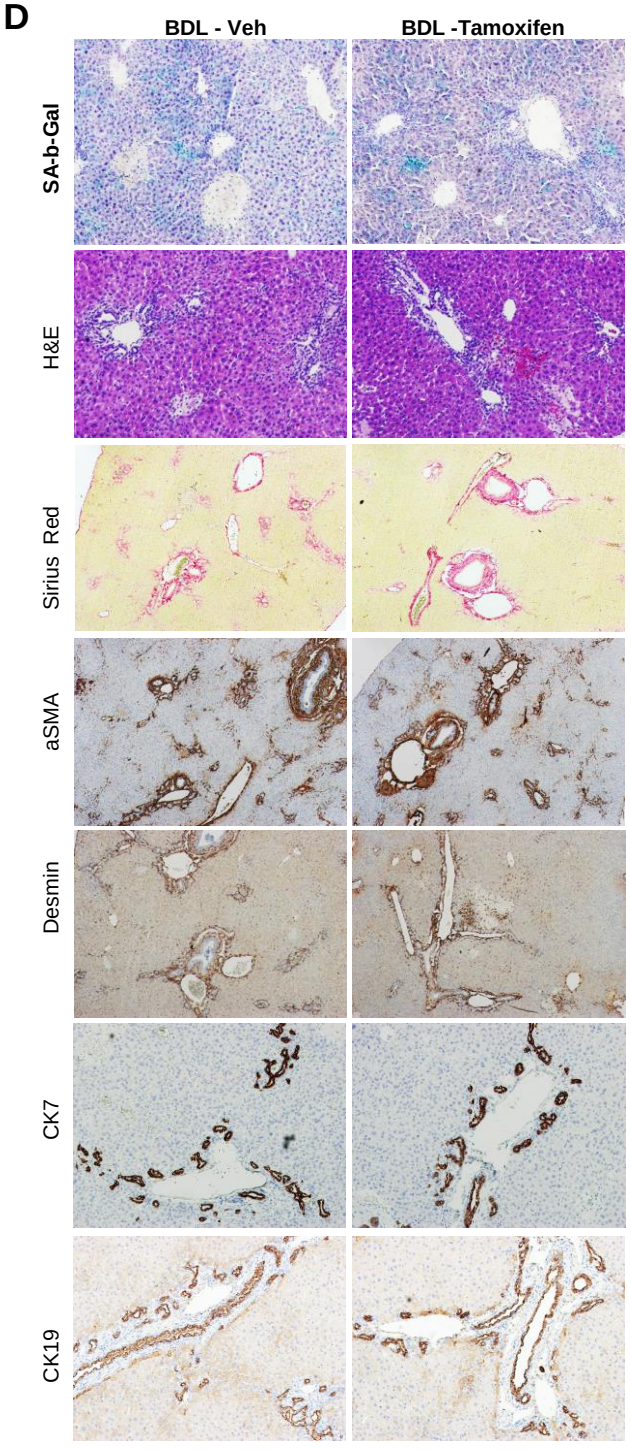

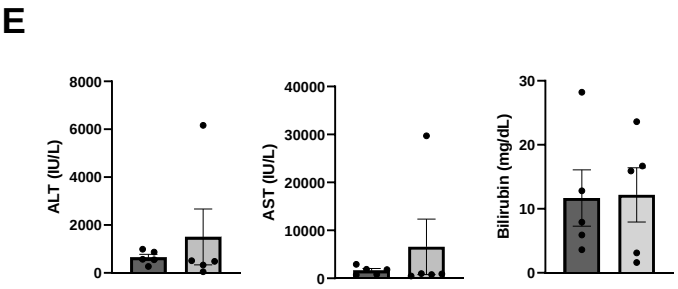

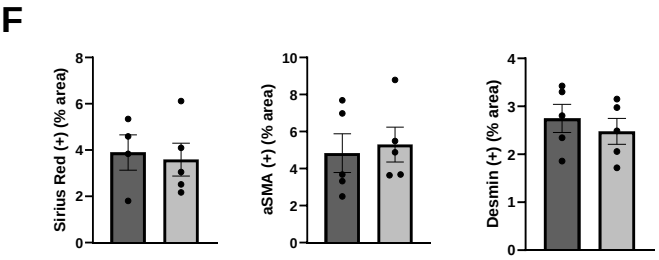

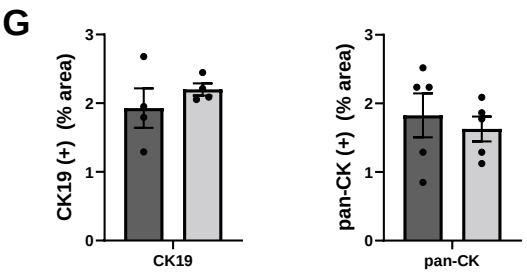

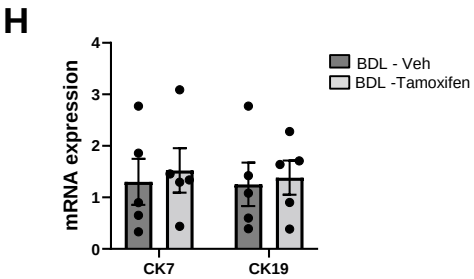

Suppl. Fig 14. Selective Yap1 deletion caused HSC senescence and reduced liver injury and fibrosis in MCD fed mice

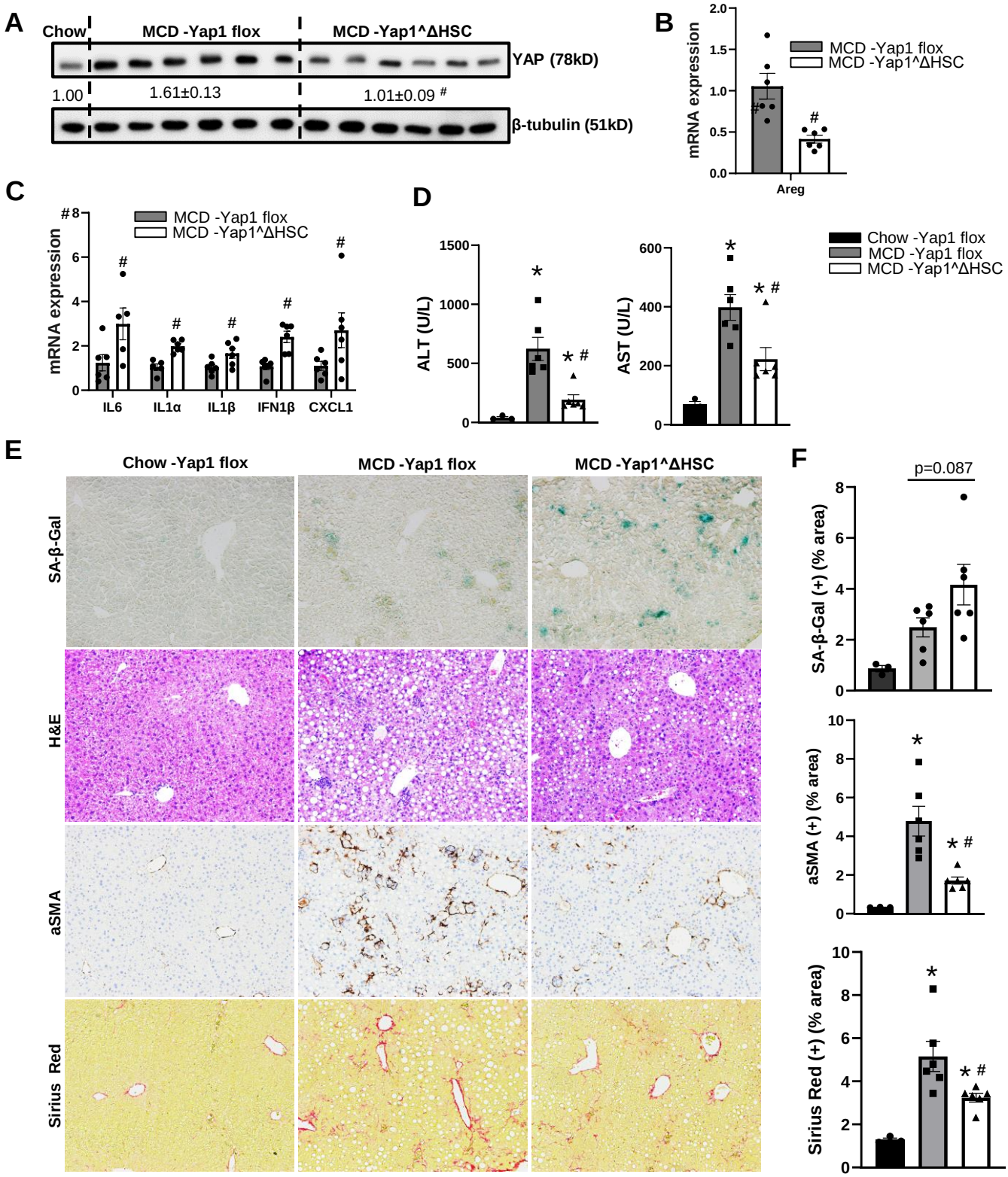

Suppl. Fig. 15 Selective Yap1 deficiency in HSCs in fibrotic mice also dramatically changed gene signatures involved in fibrogenesis, cell cycle, senescence, apoptotic and ferroptoic pathways.

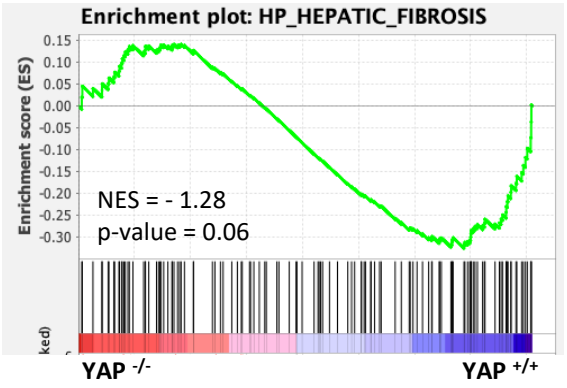

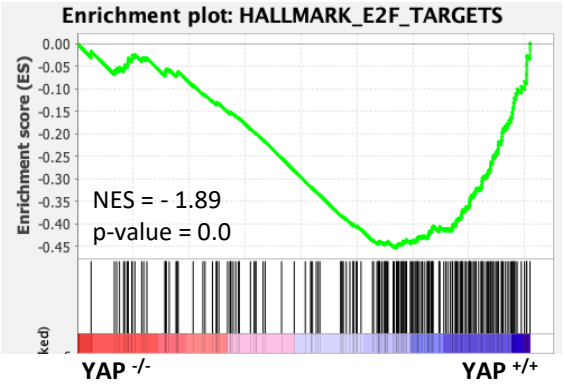

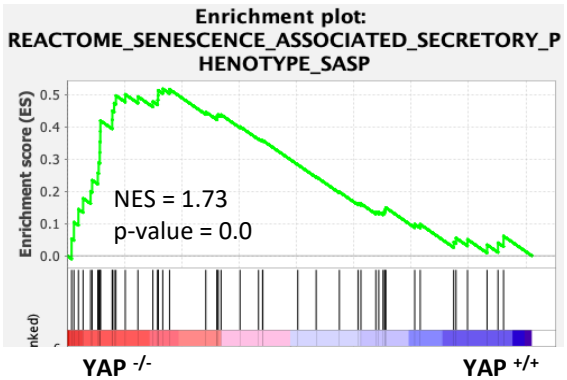

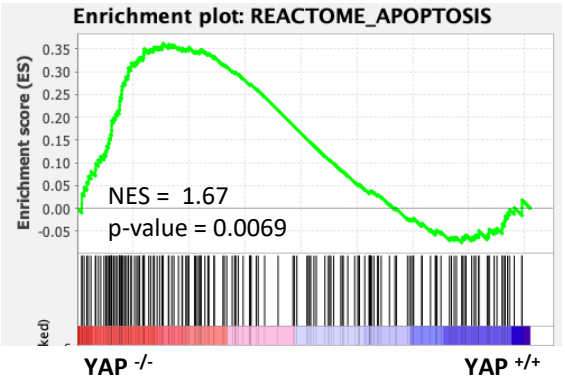

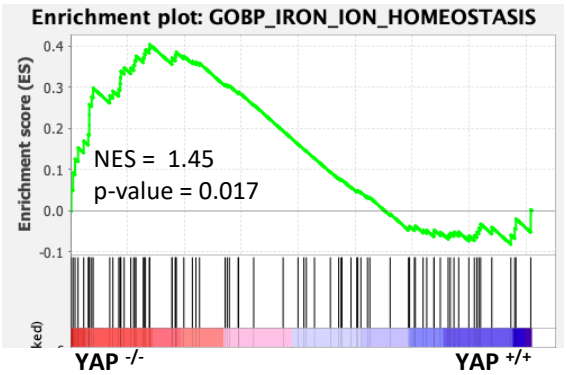

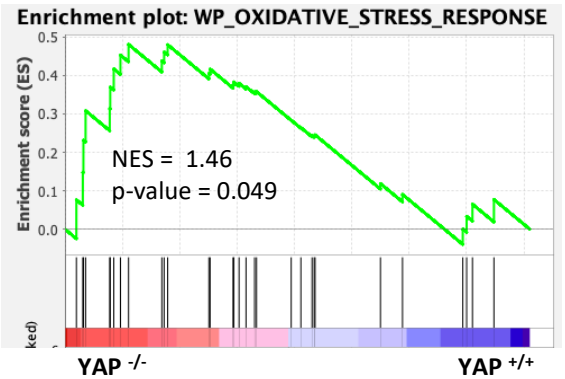

Abbreviations used in this paper: αSMA, alpha-smooth muscle actin; ACTA2, actin alpha 2; ALT, alanine aminotransferase; AST, aspartate aminotransferase; BDL, bile duct ligation; CCK8, cell counting kit 8; DMSO, dimethyl sulfoxide; ECM, extracellular matrix; FBS, fetal bovine serum; GPX4, glutathione peroxidase 4; GSEA, Gene Set Enrichment Analysis; GSH, glutathione; H&E, Haemotoxylin and Eosin; Hep, hepatocyte; HSC, hepatic stellate cell; ICC, immunocytochemistry; IF, immunofluorescence; IHC, immunohistochemistry; i.p. intraperitoneal; Lip-1, liproxstatin-1; MCD, methionine-choline deficient; MF, myofibroblast; MF-HSC, myofibroblastic hepatic stellate cell; NAC, N-acetyl cysteine; pHSC, primary hepatic stellate cell; Q-HSC, quiescent hepatic stellate cell; qRT-PCR, quantitative reverse-transcription polymerase chain reaction; ROS, reactive oxidative stress; SASP, senescence-associated secretory phenotype; TAZ, WW domain-containing transcription regulator protein 1; TUNEL, terminal deoxynucleotidyl transferase (TdT) dUTP Nick-End Labeling; VIM, vimentin; YAP, yes associated protein

Reference

1. Hao Y, Hao S, Andersen-Nissen E, Mauck WM, 3rd, Zheng S, Butler A, Lee MJ, et al. Integrated analysis of multimodal single-cell data. Cell 2021;184:3573-3587 e3529.
2. Borcherding N, Vishwakarma A, Voigt AP, Bellizzi A, Kaplan J, Nepple K, Salem AK, et al. Mapping the immune environment in clear cell renal carcinoma by single-cell genomics. Communications biology 2021;4:1-11.
3. Bunis DG, Andrews J, Fragiadakis GK, Burt TD, Sirota M. dittoSeq: universal user-friendly single-cell and bulk RNA sequencing visualization toolkit. Bioinformatics 2021;36:5535-5536.
4. Kim D, Langmead B, Salzberg SL. HISAT: a fast spliced aligner with low memory requirements. Nat Methods 2015;12:357-360.
5. Anders S, Pyl PT, Huber W. HTSeq--a Python framework to work with high-throughput sequencing data. Bioinformatics 2015;31:166-169.
6. Love MI, Huber W, Anders S. Moderated estimation of fold change and dispersion for RNA-seq data with DESeq2. Genome Biol 2014;15:550.
7. Subramanian A, Tamayo P, Mootha VK, Mukherjee S, Ebert BL, Gillette MA, Paulovich A, et al. Gene set enrichment analysis: a knowledge-based approach for interpreting genome-wide expression profiles. Proc Natl Acad Sci U S A 2005;102:15545-15550.
8. Mootha VK, Lindgren CM, Eriksson KF, Subramanian A, Sihag S, Lehar J, Puigserver P, et al. PGC-1alpha-responsive genes involved in oxidative phosphorylation are coordinately downregulated in human diabetes. Nat Genet 2003;34:267-273.
9. Du K, Oh SH, Dutta RK, Sun T, Yang WH, Chi JT, Diehl AM. Inhibiting xCT/SLC7A11 induces ferroptosis of myofibroblastic hepatic stellate cells but exacerbates chronic liver injury. Liver Int 2021;41:2214-2227.
10. Shang L, Hosseini M, Liu X, Kisseleva T, Brenner DA. Human hepatic stellate cell isolation and characterization. J Gastroenterol 2018;53:6-17.
11. El Taghdouini A, Najimi M, Sancho-Bru P, Sokal E, van Grunsven LA. In vitro reversion of activated primary human hepatic stellate cells. Fibrogenesis Tissue Repair 2015;8:14.
12. Friedman SL, Rockey DC, McGuire RF, Maher JJ, Boyles JK, Yamasaki G. Isolated hepatic lipocytes and Kupffer cells from normal human liver: morphological and functional characteristics in primary culture. Hepatology 1992;15:234-243.
13. Balaphas A, Meyer J, Gameiro C, Frobert A, Giraud MN, Egger B, Buhler LH, et al. Optimized Isolation and Characterization of C57BL/6 Mouse Hepatic Stellate Cells. Cells 2022;11.